Bull Math Biol (2014) 76:157–183
DOI 10.1007/s11538-013-9914-6

Society for Mathematical Biology

ORIGINAL ARTICLE

An Efficient, Nonlinear Stability Analysis for Detecting Pattern Formation in Reaction Diffusion Systems

William R. Holmes

Received: 5 February 2013 / Accepted: 8 October 2013 / Published online: 25 October 2013

Abstract Reaction diffusion systems are often used to study pattern formation in biological systems. However, most methods for understanding their behavior are challenging and can rarely be applied to complex systems common in biological applications. I present a relatively simple and efficient, nonlinear stability technique that greatly aids such analysis when rates of diffusion are substantially different. This technique reduces a system of reaction diffusion equations to a system of ordinary differential equations tracking the evolution of a large amplitude, spatially localized perturbation of a homogeneous steady state. Stability properties of this system, determined using standard bifurcation techniques and software, describe both linear and nonlinear patterning regimes of the reaction diffusion system. I describe the class of systems this method can be applied to and demonstrate its application. Analysis of Schnakenberg and substrate inhibition models is performed to demonstrate the methods capabilities in simplified settings and show that even these simple models have nonlinear patterning regimes not previously detected. The real power of this technique, however, is its simplicity and applicability to larger complex systems where other nonlinear methods become intractable. This is demonstrated through analysis of a chemotaxis regulatory network comprised of interacting proteins and phospholipids. In each case, predictions of this method are verified against results of numerical simulation, linear stability, asymptotic, and/or full PDE bifurcation analyses.

Keywords Reaction diffusion · Pattern formation · Nonlinear stability analysis · Local perturbation analysis

W.R. Holmes (✉)
Department of Mathematics, University of California Irvine, Irvine, CA, USA
e-mail: wrholmes@uci.edu

1 Introduction

Reaction diffusion equations (RDEs) have provided a ubiquitous framework for studying pattern formation in chemical and biological systems (Turing 1952; Gierer and Meinhardt 1972; Lewis and Kareiva 1993; Murray 2002; Jilkine et al. 2007; Goehring et al. 2011). As a result of their sustained interest, numerous linear (Turing 1952), weakly nonlinear (Pismen and Rubinstein 1999; Short et al. 2010; Rubinstein et al. 2012; Kaper et al. 2009; van der Stelt et al. 2013), and fully non-linear (Iron and Ward 2000; Kolokolnikov et al. 2005a, 2005b, 2005c; Ward and Wei 2002; Ueda and Nishiura 2012; Mori et al. 2011; Doelman et al. 1998, 2007; Doelman and Veerman 2012; Veerman and Doelman 2013) techniques for analyzing RDEs have been developed. Here, I present an efficient, relatively simple addition to this toolbox, aimed at analyzing systems where diffusivities are substantially different.

A difference in rates of diffusion has been implicated as being of vital importance for patterning in numerous biological systems. In the context of cell biology, some rates of diffusion are not just different but are vastly different, varying by factors of 100–1000. Numerous cell functions are controlled by regulators, such as "GTPase's" in cell motility (Jilkine et al. 2007; Holmes et al. 2012a, 2012b; Dawes and Edelstein-Keshet 2007; Marée et al. 2006; Mori et al. 2008), "ROP's" in plant development (Fu and Yang 2001), and "Min" proteins in bacterial division (Huang et al. 2003; Huang and Wingreen 2005). All of these regulatory proteins have fast and slow diffusing components since they exist in membrane bound and unbound states. Analysis of these types of systems motivated the development of this method.

Here, I consider a generic system of RDEs with a large diffusion disparity and highlight a useful method for understanding their linear and nonlinear stability properties. Consider the following generic system:

$$\frac{\partial u}{\partial t}(x,t) = f(u,v;p) + \mathbf{D_u} u_{xx}, \tag{1a}$$

$$\frac{\partial v}{\partial t}(x,t) = g(u,v;p) + \mathbf{D_v} v_{xx}, \tag{1b}$$

where u and v are vectors, $\mathbf{D_u}, \mathbf{D_v}$ are diagonal matrices of diffusion coefficients, and p is a vector of reaction parameters. We will assume for $(u,v) \sim O(1)$, f and g are $O(1)$ so that the timescale of reaction kinetics is $O(1)$. We will further assume that the diagonal entries of $\mathbf{D_u}$ (resp. $\mathbf{D_v}$) are small (resp. large) and refer to u and v as "slow" and "fast" variables respectively. The essential point moving forward is that this produces a three timescale problem with slow, intermediate, and fast timescales related to u diffusion, reactions, and v diffusion. We will exploit this feature to simplify the analysis of this system.

The "Local Perturbation Analysis" (LPA) is a nonlinear stability technique applicable to systems of this type. This method, originally devised by Grieneisen (2009), is a bridge between linear and nonlinear analysis methods having benefits of each. Linear stability analysis (Turing 1952) is straightforward and widely used, but is limited to providing linear information. Nonlinear methods, while more informative, are much more challenging, often specific to the system being investigated, usually require an ansatz or a priori knowledge of the solution being investigated, and rarely

scale up to complex systems with many variables. Recent advances (Veerman and Doelman 2013; Doelman and Veerman 2012) have led to more general techniques that are less sensitive to the specifics of the system, but they are still limited to low dimensional systems (e.g., (2a)–(2c)). The LPA provides nonlinear stability information beyond that of linear stability analysis, but is relatively simple to implement. An important consequence of this simplicity is that it can be readily applied to complex systems involving many variables where other methods become intractable (see Sect. 5).

In contrast to linear stability analysis which probes stability of a homogeneous steady state (HSS) with respect a small amplitude, spatially extended perturbation, the LPA probes stability with respect to a spatially localized, large amplitude perturbation of the slow variable u. As will be shown, when diffusion of u (resp. v) is sufficiently slow (resp. fast) the perturbed region and broader domain evolve according to an approximate collection of ODE's on the timescale of reactions

$$\frac{du^g}{dt}(x,t) = f\big(u^g, v^g; p\big), \tag{2a}$$

$$\frac{dv^g}{dt}(x,t) = g\big(u^g, v^g; p\big), \tag{2b}$$

$$\frac{du^l}{dt}(x,t) = f\big(u^l, v^g; p\big). \tag{2c}$$

The variables (u^g, v^g) represent "global" concentrations away from the perturbation and u^l the concentration at the local perturbation. Tracking the growth or decay of this perturbation provides stability information for (1a), (1b). There are three primary benefits to this technique that make it an ideal complement to existing techniques:

(1) The large amplitude "probe" detects pattern formation in linearly stable parameter regimes,
(2) In these nonlinear patterning regimes, the analysis results provide qualitative information about the dependence of "response thresholds" on system parameters,
(3) It is scalable to large, complex systems involving potentially large numbers of interacting components. Further its application is not highly specific to the particular system being investigated and its implementation takes advantage of existing software.

Applications of this method to biologically motivated reaction diffusion systems are found in Mata et al. (2013), Holmes et al. (2012a, 2012b), Grieneisen (2009). Rather than focus on a specific phenomena or biological system, my goal here is to explain and validate the method itself. I will describe the types of RDEs to which this method is applicable, its limitations, and the type of information that it can (and cannot) provide. Well-known examples of pattern forming systems are used to demonstrate its application and make direct comparisons between its predictions and results of classical methods (e.g., linear stability analysis, full PDE bifurcation, or numerical simulation). In the context of a more complex chemotaxis related example, I also show this method: Easily scales to larger systems with many variables, allows the user to gain a more complete overview of the parameter space structure than with

other methods, and greatly aids investigation of both parametric and structural perturbations of a complex reaction network.

2 Local Perturbation System Formulation

I now proceed to show that the evolution of a spatially localized perturbation of a homogeneous steady state of Eqs. (1a), (1b) evolves according to Eqs. (2a)–(2c). Consider Eqs. (1a), (1b) on the interval $[-1, 1]$ with no flux boundary conditions, and u, v in $\mathbb{R}^M$ and $\mathbb{R}^N$, respectively. It is not necessary to assume all slow (respectively fast) variables have the same diffusivities, only that they can be divided into fast and slow diffusing classes. For notation simplicity, however, assume

$$\mathbf{D_u} = \epsilon^2 \mathbb{I}, \qquad \mathbf{D_v} = D\,\mathbb{I}, \tag{3}$$

where $\mathbb{I}$ is the properly sized identity matrix. The central assumption will be that the three timescales defined by reaction kinetics, slow, and fast diffusion respectively are substantially different, i.e. $\epsilon^2 \ll 1 \ll D$. Nondimensionalization by domain size and the reaction timescale (so that $f, g \sim O(1)$) have been implicitly assumed. Further assume this system has a HSS (u^s, v^s) satisfying $f(u^s, v^s; p) = 0 = g(u^s, v^s; p)$.

Consider a highly localized perturbation of this steady state of the form

$$\begin{aligned} u(x,0) &= u^s, \qquad v(x,0) = v^s, \quad |x| > \sqrt{\epsilon}, \\ u(x,0) &= u^p, \qquad v(x,0) = v^p, \quad |x| < \sqrt{\epsilon}, \end{aligned} \tag{4}$$

where (u^p, v^p) is $O(1)$ with respect to ϵ and D; see Fig. 1. Denote R^l to be the local region $|x| < \sqrt{\epsilon}$ and R^g the global region $|x| > \sqrt{\epsilon}$.

2.1 Time and Space Scale Separation

To track the evolution of (u, v) on these regions, different time and space scales must be considered. A multiple timescale argument is applied to parse the role of reaction and diffusion effects on different timescales, and a transition/boundary layer technique is used to separate relevant space scales.

The reaction, slow, and fast diffusion timescales inherent in this class of RDE's can be described by $t = O(1)$, $t_u = \epsilon^2 t$, and $t_v = Dt$, with the intermediate reaction timescale of most interest here. Suppose $u = U(x, t, t_u, t_v)$, $v = V(x, t, t_u, t_v)$. With the perturbation (4) taken as an initial condition, transition layers on an $O(\epsilon)$ length scale are expected; see dashed lines in Fig. 1. Employing a stretched coordinate $\xi = (x - x_{\text{layer}})/\epsilon$ near transition layers, we come to two systems:

$$\frac{\partial U}{\partial t} = f + \epsilon^2 U_{xx}, \qquad \frac{\partial V}{\partial t} = g + DV_{xx} \tag{5}$$

describing outer regions away from transition layers and

$$\frac{\partial U}{\partial t} = f + U_{\xi\xi}, \qquad \frac{\partial V}{\partial t} = g + \frac{D}{\epsilon^2} V_{\xi\xi}, \tag{6}$$

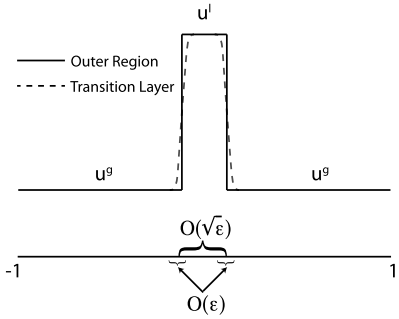

Fig. 1 To probe nonlinear stability, the local perturbation analysis probes the response of a homogeneous steady state of Eqs. (1a), (1b) to a localized perturbation Eq. (4). To leading order, values in the perturbed region (R^l) and the broader domain (R^g), denoted u^l, u^g, respectively, will evolve independently. The fast variable v, not depicted here, will be spatially uniform on the entire domain taking value v^g. Transition layer effects are present on $O(\epsilon)$ regions, but to leading order do not influence evolution of the perturbation. A collection of ordinary differential equations for (u^g, v^g, u^l) describe the growth or decay of this perturbation and provide stability information for (1a), (1b)

describing dynamics in transition layers. I now describe the evolution of (U, V) on the outer regions $R^{g,l}$ on the short and intermediate timescales.

2.2 Evolution on the Fast Diffusion Timescale

Consider first the fast diffusion timescale and assume U, V are described by first-order perturbative expansions $U = U^0 + \epsilon U^1$, $V = V^0 + \epsilon V^1$. Substituting $t_v = Dt$ into Eq. (5) and collecting leading order terms

$$\frac{\partial U^0}{\partial t_v} = 0, \qquad \frac{\partial V^0}{\partial t_v} = V^0_{xx}, \tag{7}$$

it is clear that in outer regions, $U^0 = U^0(x, t, t_u)$ does not evolve due to either reaction or diffusion and V^0 simply spreads due to diffusion

$$V^0(x, t, t_u, t_v) = v^0(t, t_u) + \sum_{n=1}^{\infty} v^n(t, t_u) \exp\left(-(n\pi)^2 t_v\right) \cos(n\pi x). \tag{8}$$

So in each outer region $R^{l,g}$, V^0 evolves to a constant value exponentially quickly with t_v.

Thus, (U^0, V^0) will evolve to a piecewise constant profile with possibly different values in R^g and R^l; see Fig. 1. Denote the values on the global domain R^g by (u^g, v^g) and those on the local region R^l as (u^l, v^l). Now consider the transition layers between these regions on this fast timescale. Given the spatial symmetry, consider only the left transition layer and substitute $t_v = Dt$ into Eq. (6). $O(\epsilon^{-2})$ terms indicate that $V^0_{\xi\xi} = 0$. Thus, to leading order

$$V^0 = a_0(t_v)\xi + a_1(t_v).$$

Matching conditions dictate that

$$\lim_{\xi\to\infty} V^0(\xi) = v^l, \qquad \lim_{\xi\to-\infty} V^0(\xi) = v^g.$$

So, $a_0 = 0$, resulting in a shadow system (Nishiura 1982; Li and Ni 2009) where V^0 is constant over the entire domain. Its value will be denoted $v^g(t, t_u)$. On this timescale to leading order, $U^0_{t_v} = 0$ so that transition layer effects do not influence U^0.

2.3 Evolution on the Intermediate Reaction Timescale

Evolution of this perturbation on the reaction timescale will determine the stability of the HSS. As t_v progresses approaching this timescale, to leading order the solution in the outer regions is described by (u^g, v^g, u^l), representing the piecewise constant values on $R^{l,g}$, respectively. The evolution of these values on this timescale are described by Eq. (5) with $t = O(1)$. To leading order

$$\frac{\partial U^0}{\partial t} = f\big(U^0, V^0; p\big), \qquad \frac{\partial V^0}{\partial t} = g\big(U^0, V^0; p\big). \tag{9}$$

Substituting (u^g, v^g) and (u^l, v^g) respectively into the first of these, we obtain Eqs. (2a), (2c). Integrating the evolution equation for V^0 in Eq. (9) over the domain, we see that

$$\frac{\partial v^g}{\partial t} = \frac{1}{2}\int_{-1}^{1} g\big(U^0, v^g; p\big)\,dx = g\big(u^g, v^g; p\big) + \sqrt{\epsilon}\big[g\big(u^l, v^g; p\big) - g\big(u^g, v^g; p\big)\big]. \tag{10}$$

So, to leading order the values (u^l, u^g, v^g) evolve according to (2a)–(2c) on the intermediate timescale. Equations (2a)–(2c) will be referred to as the LPA system of ODE's (or LPA–ODE's) associated with Eqs. (1a), (1b). Diffusion and transition layer effects become important on the slow timescale, so evolution of any perturbation beyond the intermediated timescale requires consideration of features specific to the system being investigated.

A few remarks about the LPA–ODE's (Eqs. (2a)–(2c)) are in order at this point. First, they represent a singular limit of the original RDE's in Eqs. (1a), (1b). The consequence of this is that the evolution of u on the broader domain (represented by u^g) is independent of u^l since diffusive coupling is gone ($\epsilon \to 0$) and the effect of u^l on the fast variable is negligible. This is evident in the structure of Eqs. (2a)–(2c) where Eqs. (2a), (2b) decouple completely from (2c). In fact, (2a), (2b) represent the canonical "well mixed" system associated with Eqs. (1a), (1b). Implications of this decoupling are briefly mentioned in Sect. 3 and discussed in detail in Sects. 3.1 and 4.

3 The Local Perturbation Analysis: Application and Examples

The goal of the LPA is to determine in which parameter regimes localized perturbations of this form grow or decay. Growth suggests a patterning response and decay back to the HSS suggests stability. Since the evolution of this perturbation is described by Eqs. (2a)–(2c), the location and stability of its steady states/fixed points

provides predictions about the stability properties of the HSS of Eqs. (1a), (1b). This information can be found using standard bifurcation analysis techniques for systems of ODEs.

In coming sections, I will demonstrate this method through example and the following capabilities will be emphasized.

(1) The LPA detects linear instabilities of Eqs. (1a), (1b). In future discussions, we distinguish two types of linear instabilities, well mixed instability (to a spatially homogeneous perturbation) and Turing instability (to heterogeneous perturbations). The detection of well mixed instabilities is a direct consequence of the Eqs. (2a), (2b) precisely representing the well mixed system. Detection of Turing instabilities will be the subject of Theorem 4.1 in Sect. 4.
(2) The LPA detects inherently nonlinear patterning where a HSS is linearly stable, but a sufficiently large perturbation yields a patterning response.
(3) While the LPA approximation is not valid on the slow timescale of pattern evolution, its results can be used to make reasonable conjectures about the type of pattern (i.e., highly localized spike or a sharp interface separating distinct planer regions) that might evolve.
(4) In nonlinear patterning regimes, the LPA qualitatively maps the dependence of patterning response thresholds on system parameters p (excluding diffusion parameters).

The LPA is applied to two classical systems, Schnakenberg (1979) and Substrate Inhibition (Kernevez et al. 1979), both well studied in Murray (1982), Ward and Wei (2002), Iron et al. (2004), for example. Predictions of this analysis are then directly compared to results of linear stability, numerical, full PDE bifurcation, and asymptotic analyses.

3.1 The Local Perturbation Analysis of a Schnakenberg Model

The Schnakenberg system is a Turing model where u is an activator and v a substrate.

$$u_t(x,t) = a - u + u^2 v + \epsilon^2 \Delta u = f(u,v) + \epsilon^2 \Delta u, \tag{11a}$$

$$v_t(x,t) = b - u^2 v + D\Delta v = g(u,v) + D\Delta v. \tag{11b}$$

u decays linearly, both are produced uniformly in the domain, and the nonlinearity represents an autocatalytic reaction where u consumes v. A linear stability analysis of Eqs. (11a), (11b) can be found in Murray (1982). In Ward and Wei (2002), Iron et al. (2004), asymptotic and spectral analysis showed that for $a = 0$, highly localized spike solutions exist and are stable.

It is possible to analytically perform the LPA for Eqs. (11a), (11b). The resulting system of LPA–ODE's becomes

$$u_t^g = a - u^g + \left(u^g\right)^2 v^g, \tag{12a}$$

$$v_t^g = b - \left(u^g\right)^2 v^g, \tag{12b}$$

$$u_t^l = a - u^l + \left(u^l\right)^2 v^g. \tag{12c}$$

Here, $p = (a, b)$ is the vector of system parameters and a will be the bifurcation parameter of interest. Equations (12a), (12b) decouple from Eq. (12c) and simply represent the spatially homogeneous, well mixed system (i.e., with $\epsilon = 0 = D$). The unique HSS (u^s, v^s) of Eqs. (11a), (11b)

$$u^s = a + b, \qquad v^s = \frac{b}{(a+b)^2}, \tag{13}$$

is thus a solution of Eqs. (12a), (12b). Similarly $(u^g, v^g, u^l) = (u^s, v^s, u^s)$ is a steady state of Eqs. (12a)–(12c). This steady state of the LPA–ODE's represents the HSS of Eqs. (11a), (11b) with no perturbation, i.e., both $u^{l,g} = u^s$.

While this is the only HSS of the RDE system, the LPA system actually has two steady states with the second satisfying

$$u^g = u^s, \qquad v^g = v^s, \qquad u^l = a + \frac{a^2}{b} =: u^{l1}. \tag{14}$$

With b fixed and a considered as a bifurcation parameter, the steady state branches u^s and u^{l1} intersect in a transcritical bifurcation at $a = b$. Furthermore, it can be readily shown by computing the Jacobian of Eqs. (12a)–(12c) that the stability of these branches is determined solely by the sign of f_u and that

$$\frac{\partial f}{\partial u}\left(u^s, v^s\right) > 0, \qquad \frac{\partial f}{\partial u}\left(u^{l1}, v^s\right) < 0, \quad a < b, \tag{15}$$

$$\frac{\partial f}{\partial u}\left(u^s, v^s\right) < 0, \qquad \frac{\partial f}{\partial u}\left(u^{l1}, v^s\right) > 0, \quad a > b. \tag{16}$$

The location and stability of these steady states is depicted in Fig. 2a. The HSS branch $(u^g, v^g, u^l) = (u^s, v^s, u^s)$ is linearly unstable for $a < 1$ (Region I). For $a > 1$ (Region II), the HSS is linearly stable, however a perturbation of u^l above the u^{l1} branch will grow to infinity. From here on, the HSS branch $(u^g, v^g, u^l) = (u^s, v^s, u^s)$ will be referred to as a "global" steady state branch of the LPA system. $(u^g, v^g, u^l) = (u^s, v^s, u^{l1})$ will be referred to as a "local" branch, since it describes a steady state of the local variable u^l.

3.1.1 Local Perturbation Analysis Predictions

These results lead to the following predictions.

Prediction 1: A Turing bifurcation occurs near $a = 1$. For $a < 1$, the homogeneous steady state of Eqs. (11a), (11b) is linearly unstable. For $a > 1$, it is stable but sufficiently large perturbations yield a patterning response.

Based on the asymptotics above, it is expected that the initial behavior of a local perturbation of the RDE's mimics the behavior of the perturbation u^l determined by this bifurcation analysis. In region I ($a < 1$ in Fig. 2a), arbitrarily small perturbations of $u^l = u^s$ grow, predicting the HSS of Eqs. (11a), (11b) is linearly unstable. In region II, sufficiently large perturbations of u^l are required to elicit a response for

the LPA–ODE's, suggesting the HSS is linearly stable but large perturbations yield a response.

Prediction 2: In region II, as a increases, increasingly large perturbations are required to initiate patterning.

In region II ($a > 1$), the gap between the stable global and unstable local branches represents a response threshold for the LPA–ODE's: a perturbation of u^l below the threshold decays back to the global HSS branch, a perturbation above it grows. The dependence of this response threshold on the system parameter a can be found by visual inspection of the LPA diagram. For $a > 1$, that threshold increases with a. This threshold is precise only in the $\epsilon \to 0, D \to \infty$ limit, however the qualitative dependence on a is expected to hold for the RDE system (11a), (11b) with sufficiently extreme diffusivities.

Prediction 3: The predicted Turing bifurcation near $a = 1$ is *sub-critical* for sufficiently extreme diffusivities with large amplitude patterned states present on both sides of the bifurcation.

In dynamical systems theory, the terms *subcritical* and *super-critical* are often used to describe the character of bifurcations such as Hopf or pitchfork. Super-critical denotes a bifurcation that gives rise to a small amplitude response upon crossing it. Subcritical denotes one where the HSS loses stability immediately giving way to a large amplitude response. In the latter case, responses can occur even outside of the unstable regime given a sufficient perturbation. The Turing bifurcation near $a = 1$ is predicted to be subcritical with the unstable local branch u^{l1} characterizing a threshold that shrinks to 0 at the bifurcation, giving rise to instability of the HSS.

Prediction 4: Predicted patterned solutions take the form of a spatially localized spike for sufficiently distinct diffusivities.

In region II, the LPA–ODE's exhibit blow up; a perturbation above the critical threshold grows to infinity. When this perturbation becomes large, diffusion is expected to become important for the RDEs. This will tend to oppose growth and smooth the solution. It is reasonable to conjecture that at a particular height, reaction driven growth, and diffusion driven suppression will balance leading to a large amplitude, spatially localized spike. For future reference, it is expected that when ϵ decreases, decreasing the strength of diffusion, this spike would be come taller and more localized.

3.1.2 Confirmation of Predictions

Figures 2b, 2c, 2d show results of linear stability, full PDE bifurcation, and numerical analyses for Eqs. (11a), (11b). These results confirm the predictions above with a few caveats discussed at the end of this section.

Confirmation of Prediction 1 Results of a Turing stability analysis in Fig. 2b confirm the presence of a linear instability for $a < 1$. There, eigenvalues of the linearized Jacobian (i.e., Turing growth rates) are plotted as a function of the bifurcation parameter a for four successively smaller values of ϵ. For $a \lesssim 1$, there is a positive Turing

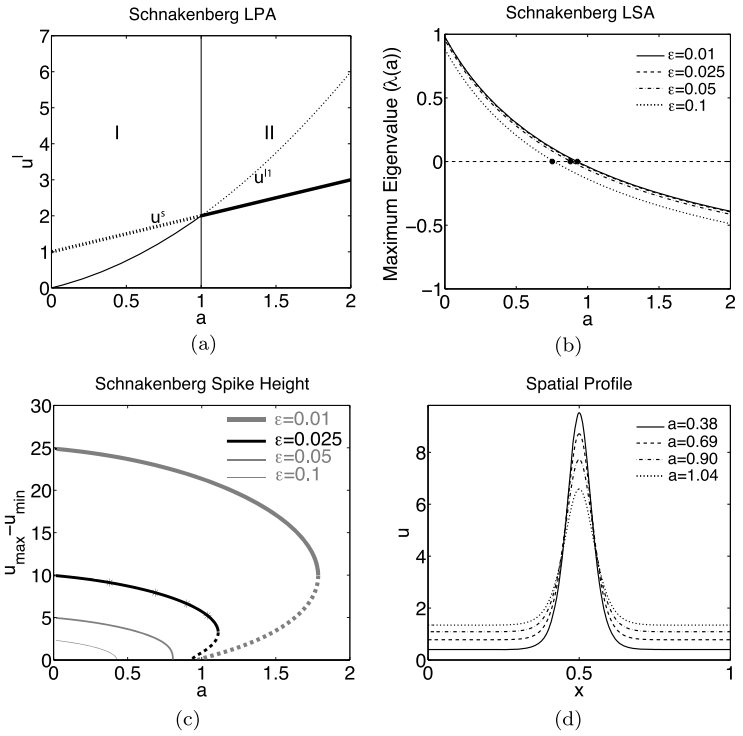

Fig. 2 Comparison of linear stability, local perturbation, and full PDE bifurcation analysis results for the Schnakenberg system (Eqs. (11a), (11b)). All diagrams are computed with $D = 10$, $b = 1$. (**a**) *Local perturbation analysis results*: Global u^s and local u^{I1} solution branches of Eqs. (12a)–(12c) along with their stability are plotted as a function of a. Two pattern forming regimes are predicted; (I) linearly (Turing) unstable, and (II) linearly stable where a sufficiently large perturbation induces patterning. (**b**) *Linear stability analysis (LSA) results* Maximum eigenvalue of J_1 (18) as a function of "a" for various values of ϵ. As $\epsilon \to 0$, the edge of the Turing region, marked with dots, approaches a limiting point near $a = 1$, in agreement with LPA predictions in panel *a*. (**c**) *PDE bifurcation results*: Bifurcation analysis of the full system of PDEs (Eqs. (11a), (11b)). The vertical axis describes the height (maximum − minimum) of a patterned solution. As predicted by the LPA, stable patterned solutions exist both in the linearly unstable and stable regimes for sufficiently small ϵ. The location of the Turing bifurcation near $a = 1$ agrees with panels *a,b*. Marked points represent points where the computed solution is plotted in panel *d*. (**d**) Example solutions of Eqs. (11a), (11b) with $\epsilon = 0.025$

growth rate. Dots on Fig. 2b indicate the onset of linear instability; these bifurcation values are recorded for two different values of D in Table 1. The location of these bifurcation values appears to converge to the predicted value of $a = 1$. This confirms prediction 1 and supports point 1 in Sect. 3 that the LPA detects linear instabilities.

LPA results also suggest that in the linearly stable region II, sufficiently large perturbations elicit a patterning response. To test this, both full PDE bifurcation analysis and asymptotics are employed. Figure 2c shows results of numerical continuation (using Auto (Doedel et al. 2007)) of patterned solutions of the full RDE system (Eqs. (11a), (11b)) with the vertical axis depicting the height (maximum–minimum) of the patterned solution. The horizontal axis depicts the unpatterned HSS (maximum − minimum = 0). For sufficiently small values of ϵ, the stable patterned

Table 1 Value of "a" at the edge of the Turing region for the Schnakenberg system (Eqs. (11a), (11b)) with $b = 1$ for various values of ϵ. Column two: values drawn from the marked points in Fig. 2b. Column three: similar values for $D = 1000$. The final row is the value of the bifurcation predicted by the LPA. This bifurcation approaches that predicted by the LPA as $\epsilon \to 0$, $D \to \infty$ in agreement with Corollary 4.2

ϵ	Turing ($D = 10$)	Turing ($D = 1000$)
0.1	0.76	0.82
0.05	0.88	0.95
0.025	0.91	0.98
0.01	0.93	0.99
LPA	1	1

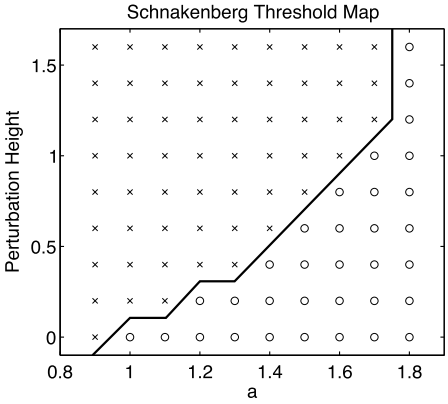

Fig. 3 Verification of the qualitative relationship between "a" and the patterning threshold in the Schnakenberg system ((11a), (11b)) using numerical simulation. $\epsilon = 0.01$ and all other parameters are as in Fig. 2. Simulations were given a period of time to settle into a stable steady state (when present). Perturbations of varying size were then applied to the middle 10 % of the domain. The *vertical axis* represents the size of the applied perturbation. "x" indicates the perturbation grows resulting in a spike. "o" indicates the perturbation decays back to the homogeneous state. The patterning threshold increases with a as indicated by the LPA. To the left $a \approx 1$, the homogeneous state is unstable and to the right of $a \approx 1.7$, it is stable to all perturbations, in agreement with Fig. 2c

solution extends into the $a > 1$ region where the HSS is linearly stable, confirming the presence of stable patterned solutions in that regime. Further, asymptotic results in Appendix A show that in the $\epsilon \to 0$, $D \to \infty$ limit, patterned solutions exist for all values of a. This confirms prediction 2 and lends support for point 2 in Sect. 3.

Confirmation of Prediction 2 In Fig. 3, local perturbations of different height were applied to the HSS for multiple values of a and the presence/absence of a pattern was recorded. As a increases, the perturbation size required to induce patterning increases as predicted by the LPA. This confirms prediction 2 and supports point 4 in Sect. 3 that results of the LPA can be used to determine the qualitative dependence of response thresholds on parameters in nonlinear patterning regimes.

Confirmation of Prediction 3 Figure 2c shows that as $\epsilon \to 0$, the nature of the Turing bifurcation changes from being super-critical to sub-critical. For large ϵ, small amplitude patterns emanate from the bifurcation. For smaller ϵ, the stable HSS gives way to large amplitude patterns immediately upon crossing the bifurcation. Also, for small ϵ, an unstable patterned state is present outside the linearly unstable regime. As the bifurcation is approached, this unstable state collapses onto the HSS changing its stability. This is similar to the standard example of a subcritical Hopf bifurcation where an unstable limit cycle colliding with a stable node results in a bifurcation.

It seems this association of a nonlinear patterning regime with a subcritical Turing bifurcation is somewhat common. Both the substrate inhibition example and the chemotaxis example in Sect. 5 presented later show subcritical bifurcations. Similarly, Rodrigues et al. (2011) observed stable heterogeneous patterns adjacent to Turing parameter regimes for a discrete predator prey model. Additionally, unpublished results show a similar parameter space structure for Doelman et al. (2007), Gray Scott Kolokolnikov et al. (2005a, 2005b) and ratio dependent predator prey (Wang et al. 2007) models.

Confirmation of Prediction 4 Figure 2d and results in Appendix A show that in both the linearly stable and unstable regimes a spike like solution forms. Furthermore, these results show that as ϵ is decreased (reducing the opposing effect of diffusion), the spike height increases as expected. Thus, the inferences in prediction 4 are confirmed in this example, supporting point 3 in Sect. 3.

3.1.3 Notes and Caveats of the Local Perturbation Results

First, it is important to note that there is no direct relationship between the solution branches in Figs. 2a, 2c. The location and stability of branches in Fig. 2a provide information about whether and under what conditions patterns "might" form. They do not provide any quantitative information about the resulting pattern, and in particular the height of the u^{l1} branch does not in any way predict the height of the resulting spike solution (which is presented in Fig. 2c.)

Second, there are discrepancies between the LPA predictions and results of linear stability and full PDE bifurcation analyses. First, the location of the predicted bifurcation at $a = 1$ is not precise. Both linear stability and PDE bifurcation results show the value of the actual Turing bifurcation depends on ϵ and D. Though this does appear to converge to the predicted $a = 1$ in the proper limit. This type of approximation error will be present in any LPA application and will be discussed in more detail in Sect. 4.

Third, the LPA predicts patterned solutions will form for all $a > 1$. Full PDE bifurcation results (Fig. 2c) in contrast show the patterned state is annihilated in a saddle node (or fold) bifurcation at a finite value of $a = a^*(b, \epsilon, D)$. The location of this bifurcation does increase as $\epsilon \to 0$ and asymptotic results in Appendix A show the presence of a patterned solution for all values of a. So in the $\epsilon \to 0, D \to \infty$ limit, $a^* \to \infty$, in agreement with LPA results. For these reasons, one must take care when interpreting the results of this analysis, recognize their limitations, and confirm them when possible.

3.2 The Local Perturbation Analysis of a Substrate Inhibition Model

I now apply the LPA to a substrate inhibition model to demonstrate a different set of results and interpretations obtained with the same method. This model (Kernevez et al. 1979)

$$u_t(x,t) = a - u - \frac{\rho u v}{1+u+Ku^2} + \epsilon^2 \Delta u = f(u,v) + \epsilon^2 \Delta u, \tag{17a}$$

$$v_t(x,t) = \alpha(b-v) - \frac{\rho u v}{1+u+Ku^2} + D\Delta v = g(u,v) + D\Delta v, \tag{17b}$$

describes two cosubstrates that are constantly generated, decay linearly, and are used up in an enzymatic reaction. The nonlinear term is indicative of multiple substrate molecules u binding to a single enzyme rendering it inert for further interaction with the remaining co-substrate v, thus the term substrate inhibition. See (Murray 1982) for linear stability results for this system.

In the previous example, it was possible to analytically compute the various solutions of the LPA system of ODEs. This will not generally be the case, but it is possible to find and track the various LPA solution branches efficiently using standard ODE bifurcation techniques. Figure 4 mirrors Fig. 2 with results in *panel b, c, d* verifying predictions inferred from LPA results in *panel a*. In this example, solution branches of the LPA–ODEs along with there stability are computed with the numerical continuation software package Matcont (Dhooge et al. 2003).

LPA results for this example predict four regimes of behavior: (I) No patterning, (II, IV) sufficiently large perturbations of the HSS lead to a patterning response, and (III) linearly (Turing) unstable. These predictions follow from the same arguments as the previous example. In region III, arbitrarily small perturbations of $u^l = u^s$ grow, suggesting instability. In region II (resp. IV), sufficiently large positive (resp. negative) valued perturbations of $u^l = u^s$ grow, suggesting a response. In region I, all perturbations of u^l decay back to u^s, suggesting the HSS is stable to all perturbations.

Result of a Turing analysis of Eqs. (17a), (17b) in Fig. 4b show that a Turing instability is present in region III as predicted, and the boundary of this regime approaches the boundary of region III as $\epsilon \to 0$, consistent with Corollary 4.2. Full PDE bifurcation analysis of Eqs. (17a), (17b) in Fig. 4c confirm the presence of patterned solutions in regions II and IV. Linear stability results show these patterns are not a result of linear instability and numerical simulation (results not shown) confirms large perturbations of HSS are required to yield patterning. Also consistent with these predictions, neither numerical continuation or simulations have revealed any patterned solutions in region I.

There are a few important contrasts between these LPA results and those for the Schnakenberg model. First, in region IV (Fig. 4a), a negative valued perturbation of the HSS is predicted to induce patterning. This along with the general dependence of response thresholds in regions II, IV were verified numerically (results not presented). Second, the LPA results suggest the resulting solution will take the form of a stable interface separating high and low regions for u.

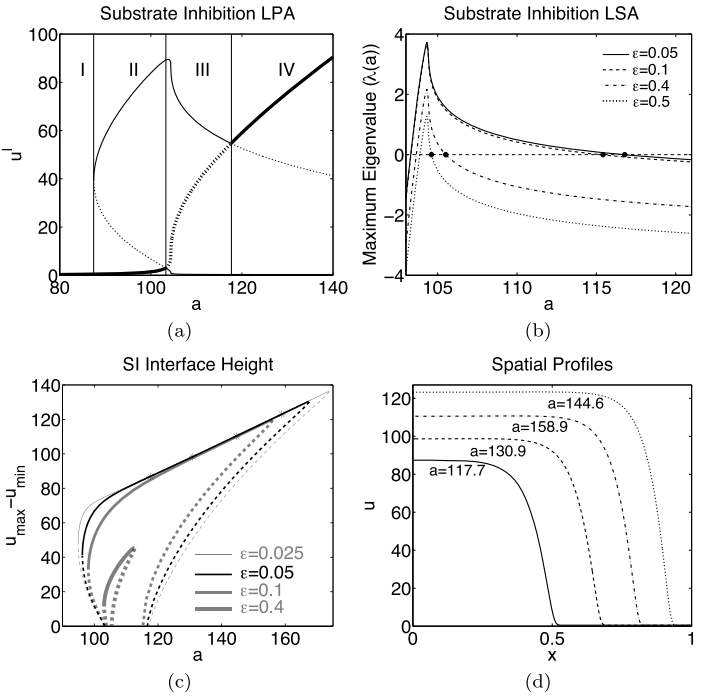

Fig. 4 Comparison of linear stability, local perturbation, and full PDE bifurcation analysis results for the substrate inhibition model (Eqs. (17a), (17b)). All diagrams are computed with $D = 10$, $\rho = 13$, $K = 0.125$, $\alpha = 1.5$, and $b = 80$ and all conventions are as in Fig. 2. (**a**) *Local perturbation analysis results*: Three regimes of behavior are predicted: No patterning (I), linearly (Turing) unstable (III), and linearly stable where a sufficiently large perturbation yields a response (II, IV). (**b**) *Linear stability analysis (LSA) results*: For each ϵ, two Turing bifurcations are seen. Dots mark the location of the right Turing bifurcation for different values of ϵ. As $\epsilon \to 0$, the edges of the Turing region approach that predicted by the local perturbation analysis results in (**a**). (**c**) *PDE Bifurcation Results*: In agreement with the LPA results, patterned solutions are found both inside and outside the linearly unstable regime. (**d**) Example solutions drawn from starred points for $\epsilon = 0.05$ in (**c**). As predicted by the LPA results, these solutions show a stable interface separating high/low regions of u

Consider region II where this system has two local branches, one unstable and the other stable. In this case, a perturbation of u^l above the unstable local branch will be attracted to the stable local branch. This suggests that a localized perturbation of the HSS in the RDE's will saturate at a specific height on the $O(1)$ reaction timescale. On longer timescales, diffusion becomes important and will cause the transition layer between the raised region and the lower background concentration to move. At this point, the region of high activity is no longer spatially localized, the asymptotic approximation breaks down (see Sect. 6 for further discussion), and the variable u^l ceases to have meaning.

We can, however, reasonably hypothesis that the resulting solution will take the form of a stable interface. The lack of a second, higher HSS suggests the high concentration region created by the perturbation cannot encompass the entire domain and one of two things will happen: (1) the transition layers will stop/stall somewhere in the interior of the domain leaving stable interfaces, or (2) the solution will eventually

collapse back to the unique HSS. LPA results can not be used to rule out the latter possibility, but results in Fig. 4d show stable interface solutions for multiple values of a. These results again support the suppositions in Sect. 3.

One final note is in order. Many nonlinear analysis techniques require initial knowledge of a solution to form a simplifying ansatz. In systems such as the Schnakenberg example, it is common to assume that the solution being investigated takes the form of a spike and the problem is reduced to finding a homoclinic orbit of a simplified equation. In cases where interface type solutions are "expected," a simplifying ansatz is used to reduce the problem to finding a heteroclinic orbit of a reduced problem. This analysis requires no such ansatz or a priori knowledge of the solutions being sought. The tradeoff of course is that results provide no rigorous information about the form of any resulting pattern.

4 Detection of Linear Instabilities by the LPA

The previous section demonstrated points 1–4 in Sect. 3. Points 2–4 relate to nonlinear patterning regimes. As with any general nonlinear result, these will likely be difficult to prove and have only been supported by the results of previous examples. The supposition in point 1 does, however, hold in generality, which is shown in this section. Since linear stability is determined by eigenvalues of an associated Jacobian, let us compare eigenvalues of the linearized RDE's to those of the linearized LPA–ODEs, which I claim have predictive value. Before continuing, let us dispense with notational definitions. Define J_k to be the Jacobian of Eq. (1a) linearized about the HSS (u^s, v^s) with respect to periodic perturbations of the form $\exp(ikx)$

$$J_k = \begin{bmatrix} f_u(u^s, v^s; p) - k^2\epsilon^2 I & f_v(u^s, v^s; p) \\ g_u(u^s, v^s; p) & g_v(u^s, v^s; p) - k^2 DI \end{bmatrix}. \tag{18}$$

Recall that $f : \mathbb{R}^M \times \mathbb{R}^N \to \mathbb{R}^M$, $g : \mathbb{R}^M \times \mathbb{R}^N \to \mathbb{R}^N$ and denote eigenvalues of this matrix as $\{\lambda_i^k(\epsilon, D, p)\}_{i=1:(M+N)}$. Assume these are in decreasing order according to their real part so that λ_1^k has the largest real part and determines stability. Further note that J_0 is precisely the Jacobian of the well-mixed system with associated eigenvalues $\{\lambda_i^0(p)\}_{i=1:(M+N)}$. Now define J_{LP} to be the linearization of the LPA–ODE's (Eqs. (2a)–(2c)) about $(u^g, v^g, u^l) = (u^s, v^s, u^s)$

$$J_{\mathrm{LP}} = \begin{bmatrix} f_u(u^s, v^s; p) & f_v(u^s, v^s; p) & 0 \\ g_u(u^s, v^s; p) & g_v(u^s, v^s; p) & 0 \\ 0 & f_v(u^s, v^s; p) & f_u(u^s, v^s; p) \end{bmatrix}. \tag{19}$$

A direct consequence of the decoupling of Eqs. (2a), (2b) from Eq. (2c) is that J_{LP} is block triangular with the upper left block being precisely J_0. Thus, J_{LP} exactly inherits all eigenvalues of the well-mixed system and as such contains all well-mixed stability information. These eigenvalues will be referred to as the well-mixed eigenvalues of J_{LP}. The remaining eigenvalues come from the lower right block $f_u(u^s, v^s)$. Denote these as $\{\lambda_j^{LP}(p)\}_{j=1:M}$ and assume they are ordered according to decreasing real part so that λ_1^{LP} has the largest real part. Then the following asymptotic result relating $\{\lambda^{LP}\}$ and $\{\lambda^k\}$ (for $k > 0$) holds.

Theorem 4.1 *Assume* $\epsilon^2 \ll 1 \ll D$, ∇f, ∇g *are* $O(1)$ *with respect to* ϵ *and* D, *and fix a wave number* $k > 0$. *Further assume that* $f_u(u^s, v^s)$, $g_v(u^s, v^s)$ *are diagonalizable. Then*:

1. *For each* $i = 1 : M$, $\lambda_i^k = \lambda_i^{LP} - k^2\epsilon^2 + c(D)$ *where* $c(D) \to 0$ *as* $D \to \infty$.
2. *For each* $i = M + 1 : M + N$, $\mathfrak{Re}(\lambda_i^k) = O^-(D)$ *where* $O^-(\,)$ *signifies a negative valued quantity of that order.*

For proof of this result, see Appendix B. A direct consequence of this is that the remaining eigenvalues of the linearized LPA–ODE's asymptotically approximate Turing growth rates ($\lambda_1^k(\epsilon, D, p) \to \lambda_1^{LP}(p)$ as $\epsilon \to 0$, $D \to \infty$) and linear instability of the HSS branch of the LPA–ODE's corresponds directly to Turing instability for the RDEs. The decoupling of Eqs. (2a), (2b) from Eq. (2c) thus separates well mixed and Turing stability information with the upper left block of Eq. (19) providing all well-mixed stability information and the bottom right block providing Turing stability information. Thus, point 1 in Sect. 3 holds for general systems of the form (1a), (1b) when $f_u(u^s, v^s)$, $g_v(u^s, v^s)$ are diagonalizable.

4.1 LPA Bifurcations Locate the Edge of "Limiting" Linearly Unstable Parameter Regimes

Recall from the linear stability results in the previous examples that the location of a Turing bifurcation of the RDE's appears to converge to a limiting point as $\epsilon \to 0$, $D \to \infty$. This is in line with Murray's (1982) observation that a linearly unstable regime of parameter space converges to a "limiting" unstable regime in this limit. As indicated by the comparison of the locations of Turing bifurcations and those predicted by the LPA, the LPA precisely locates the edge of these "limiting" unstable regimes. This is a consequence of the following corollary of Theorem 4.1.

Corollary 4.2 *Consider a particular set of parameters* p. *If the global branch of the LPA–ODE's is linearly unstable* (*i.e.*, $\mathfrak{Re}(\lambda_1^{LP}(p)) > 0$), *then the HSS of the RDE's is linearly unstable for sufficiently extreme values of* ϵ *and* D (*i.e.*, $\mathfrak{Re}(\lambda_1^k(\epsilon, D, p)) > 0$ *for some* $k > 0$). *Furthermore, if the global branch is linearly stable in the LPA sense, the HSS is linearly stable for sufficiently extreme values of* ϵ, D *as well.*

5 Applications of the LPA to More Complex Systems

One of the primary benefits of the local perturbation analysis is the relative ease with which it can be applied to more complex systems, common in biological applications. Existing methods become either difficult to implement or intractable in such cases. However, with the help of ODE analysis software packages such as Auto (Doedel et al. 2007) and Matcont (Dhooge et al. 2003), this method scales well to larger systems. The following example demonstrates an application of the LPA to a system involving 9 RDEs.

5.1 Chemotactic Polarization Example

Much effort has been devoted to understanding the process by which cells, ranging from white blood cells to cancer cells, move up chemical gradients. Reorganization of regulatory molecules, primarily GTPases and phosphoinositides, is known to be a precursor to such motion. In response to an applied chemical gradient, these molecules self organize to form a polar state where some localize in the cell "front" (Cdc42, Rac, PI3K, and PIP3) and others in the "rear" (Rho, PTEN). Front related molecules generate protrusion, rear related molecules generate contraction, and their combined activity leads to directed motion.

Each of the three GTPases (Cdc42 C, Rac R, and Rho ρ) effectively has two forms, membrane bound and cytosolic with only the membrane bound form in an active state. Over the timescale of polarization events, the amount of each GTPase is conserved with diffusion and cross talk mediated cycling between the two states leading to segregation of active forms. These cross talk interactions and the influence of phosphoinositide feedback are the focus of this discussion.

While these regulators are conserved across a wide range of eukaryotic cells, the cross talk interactions between them is not. This variation has led to extensive experimental work aimed at dissecting these interactions in different cell types and numerous models (reviewed in Jilkine and Edelstein-Keshet 2011) aimed at understanding their results. Here, I describe and analyze a variant of a model (Holmes et al. 2012b; Lin et al. 2012) motivated by work on HeLa cell polarization.

I investigate a structural perturbation of that model, introducing mutual antagonism between Rac and Rho, known to be present in numerous cell types (Sander et al. 1999; Caron 2003; van Leeuwen et al. 1997). A schematic diagram of this model is in Fig. 5a. The dashed interaction, Rho mediated inhibition of Rac, is the structural addition differentiating this model from that in (Holmes et al. 2012b; Lin et al. 2012). Model equations encoding these interactions are found in Eqs. (34a)–(34d) with a description of parameters and their values in Table 2. See Appendix C for a brief description of this model and (Holmes et al. 2012b; Lin et al. 2012) for more extensive discussion of the original network and its parameters.

What effect does the addition of Rho mediated inhibition of Rac have on the behavior of this network? To investigate this, a nondimensional parameter (f_2) modulating the strength of this inhibitory interaction is introduced. When $f_2 = 0$, no inhibition is present and the original network is recovered. When f_2 increases, the strength of the inhibition increases. LPA and numerical simulation results in Fig. 5 show the effect of increasing the strength of this feedback.

5.2 LPA and Numerical Simulation Results

Figure 5b shows the results of a LPA of this model with moderate feedback, $f_2 = 2$. The LPA was performed assuming membrane bound GTPases are slow diffusing ($D_m = 0.1$ μm^2/s), and cytosolic GTPases ($D_c = 50$ μm^2/s) are fast. For reference, cell sizes considered are on the order of 10–20 μm. Phosphoinositide diffusion lies between the fast and slow regimes. However, as in Holmes et al. (2012b), LPA results are similar with it chosen as either fast or slow. In Fig. 5, they are

taken to be slow variables. The LPA reduction in this case leads to a system of 15 ODE's for 6 local variables (C^l, R^l, ρ^l, P_1^l, P_2^l, P_3^l) and 9 global variables (C^g, R^g, ρ^g, C_c^g, R_c^g, ρ_c^g, P_1^g, P_2^g, P_3^g).

The bifurcation parameter I_{R1} represents a basal Rac activation rate. Its variation could result from either population heterogeneity or external stimulation of Rac as in Lin et al. (2012). In Fig. 5b, three regimes of behavior are found at different activation levels. For both low and high levels of basal activation, no response due to either instability or an applied stimulus can occur. For increasing levels of activation, a regime where sufficiently large perturbations yield a response is found. Again, this regime terminates in a subcritical Turing bifurcation as the response threshold shrinks to zero. This suggests increasing the spatially uniform activation rate increases the sensitivity of a cell to heterogeneous stimuli, experimentally supported in Lin et al. (2012).

At yet higher values of I_{R1}, a second narrow linearly stable patterning regime is found. Numerical simulations verify the presence of all but this narrow regime, which likely requires more extreme diffusivities to be observed numerically. LPA results again suggest solutions will evolve to a polarized profile with a transition layer separating regions of homogeneous activity levels. This was also verified numerically with an indicative steady state solution shown in the inset ($I_{R1} = 1.1$).

Now consider the effect of increasing/decreasing the strength of Rho $\dashv$ Rac feedback. Labeled branch points (BP) indicate the approximate boarder of the unstable regime. Fold bifurcations (LP) mark the boarder of the nonlinear patterning regimes. Standard two parameter continuation techniques are applied to follow these bifurcations as f_2 is varied, Fig. 5c. At low values, both regimes persist. As f_2 increases, the branch points collapse at $f_2 \sim 5$ and the linearly unstable regime between them is lost. For higher values of f_2, the two fold bifurcations of the local branch persist suggesting the continued presence of a linearly stable patterning regime between them.

Marked points on Fig. 5c indicate parameter values where numerical simulation of the full RDE system was performed. Circles indicate a parameter set where small noise (machine noise) induces a response. Points marked $\times$ indicate sufficiently large perturbations are required for a response. Beyond these points, no patterning was detected numerically at the base diffusion values. When $D_m = .01\ \mu m^2/sec$, parameter regimes expand with squares marking additional parameter sets where sufficiently large perturbations yield a response.

The linearly unstable regime for the RDE's is confined to that predicted by the LPA and as expected, stimulus induced patterning is present to the left but not to the right of that regime. While the location of patterning regimes in parameter space agree well with predictions, the expanse of these regimes is substantially smaller than predicted, particularly for the nonlinear patterning regime. However, as diffusivities are driven to yet further extremes, these regimes do expand further (results not presented).

I consider one final perturbation of this network, PI3K knockout, which is accomplished here by setting $k_{\text{PI3K}=0}$. This has the effect of removing feedback between GTPase's and phosphoinositide's. The same analysis above was performed with results in Fig. 5d. Similar parameter space structure exists with linearly unstable and stable patterning regimes. In this case, however, they are substantially compressed

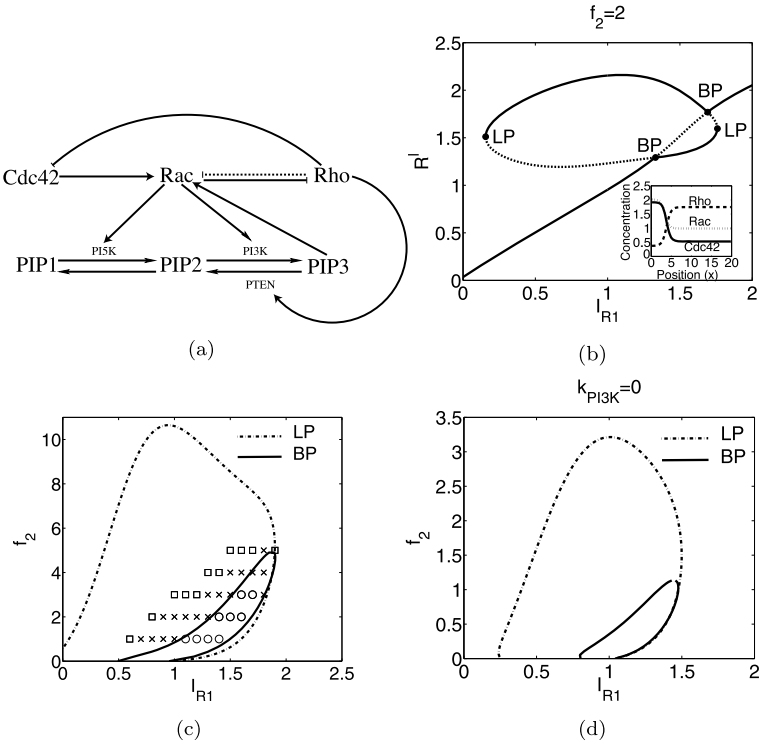

Fig. 5 (**a**) Diagram of interactions between GTPases (Cdc42, Rac, and Rho) and phosphoinositides (PIP1, PIP2, PIP3) represented by Eqs. (34a)–(34d). An *arrow* represents activation, a *bar* represents inactivation. (**b**) Local perturbation analysis of this system with $f_2 = 2$ and I_{R1} the bifurcation parameter. The *vertical axis* is the value of R^l (local form of Rac). The monotonic branch is the global branch, the loop is the local branch ordered from left to right there are four regions: no patterning, sufficiently large perturbations yield a response, linearly unstable, and no patterning. There is a small nonlinear patterning regime between $I_{R1} \sim 1.6, 1.7$, but this regime appears to only be present for extreme diffusions beyond those considered here. (*Inset*) Numerical simulation results at $f_2 = 2$, $I_{R1} = 1.1$. (**c**) Two parameter continuation of the branch points (BP), indicating the edge of a linearly unstable regime, and fold bifurcations (LP) of the local branch. Markers represent simulation results of the full RDE system. Circles indicate a Turing instability where machine noise induces patterning, "x" indicates a simulated perturbation is required for patterning, and a square indicates a parameter set for which no pattern forms at $D_m = 0.1$ but where a perturbation initiates patterning for $D_m = 0.01$. (**d**) The same as (**c**) with PI3K knockdown removing the feedback of PIP3 $\rightarrow$ Rac. See Table 2 for parameters

in parameter space. So, while PI3K/PIP3 mediated feedback is not necessary for polarization, it does make it more robust in a parametric sense. This is consistent with observations (Ferguson et al. 2006; Lin et al. 2012) showing PI3K/PIP3 localization is not necessary for efficient chemotaxis, but its knockout substantially reduces the fraction of cells that do chemotax.

6 Limitations of the LPA Approximation

Here, I stress the limitations of the local perturbation analysis. The purpose of the LPA is not to approximate a solution of Eqs. (1a), (1b) only the initial response of a

HSS to a localized perturbation (4), i.e., growth or decay. Slow diffusion timescale and transition layer effects are not considered and the LPA–ODEs (2a)–(2c) only describe the evolution of the perturbation on short to intermediate timescales. These effects can become important and the leading order approximation above can fail for one of two basic reasons.

- The perturbation becomes large. This would cause a number of effects. First, if g is unbounded, the correction term in Eq. (10) could become $O(1)$ and affect leading order dynamics. Second, if f, g are unbounded, neglected Taylor expansion terms of the form ϵf_u, ϵf_v, ϵg_u, or ϵg_v can become $O(1)$, influencing the leading order dynamics. Third, transition layer effects could influence the dynamics of (U, V) on R^l.
- The perturbation spreads in space. This would again cause the area of the perturbed region to become $O(1)$, causing the correction term in Eq. (10) to affect leading order dynamics. These effects would, however, occur on the slow diffusion timescale, which is not considered here.

In either case, these effects only become important after the perturbation has grown in amplitude, constituting a response. Given these limitations though, care should be taken when interpreting the meaning of the variable u^l. It's value represents the height of an idealized local perturbation. Once that perturbation evolves into a pattern and the asymptotic reduction breaks down, the meaning of this variable is lost. Therefore, its value provides no quantitative information about the resulting pattern.

As a result of neglecting these higher order effects, LPA predictions are asymptotic in nature and require sufficiently distinct diffusivities to be valid. Therefore, the predicted location of bifurcations between parameter regimes only approximate the location of actual bifurcations, with this approximation improving as diffusivities become more extreme. In some cases, bifurcations of the RDE system with finite diffusivities (such as the saddle node bifurcation in the Schnakenberg case) are not captured at all by the LPA.

Further, all diffusion related information is lost. Therefore, length scale information cannot be obtained, nonlinear phenomena such as peak splitting (Kolokolnikov et al. 2005b, 2005c; Barrass et al. 2006) will not be found, pattern selection, or abberent effects from domain growth, for example (Crampin et al. 1999; Barrass et al. 2006), cannot be discussed, and dependence of the resulting pattern on domain size or diffusion coefficients will not be found. For these reasons, the LPA should be viewed primarily as an efficient, scalable nonlinear stability technique, capable of detecting patterning beyond the confines where linear stability analysis is useful. It should not be viewed as a replacement for linear stability or other nonlinear PDE analysis techniques. Rather, it is a complement to them that can be used to inform further analysis when system complexity allows.

7 Discussion

A new nonlinear bifurcation technique for systems of reaction diffusion equations with large diffusion disparities (1a), (1b) was developed and demonstrated. This "Local Perturbation Analysis" (LPA) determines the response of a HSS of a system of

reaction diffusion equations to a spatially localized, large amplitude perturbation. The structure of the perturbation is not an ansatz, but is instead chosen for convenience and to aid further simplification. Under proper asymptotic assumptions about the diffusivities ϵ, D and the form of the perturbation, its evolution can be approximated to leading order by a collection of ODEs describing the perturbation (local variables) and the broader domain (global variables).

A bifurcation analysis of this collection of LPA–ODEs reveals two types of solution branches: (1) a "global" branch of solutions representing HSS solutions of the RDEs, and (2) "local" solution branches unique to the LPA–ODEs. The location and stability of the global branches provides linear stability information for the RDEs (1a), (1b). The location and stability of the local branches provides nonlinear stability information. Application of this method and interpretation of its results were demonstrated using two classical example systems, Schnakenberg and substrate inhibition. Through these examples, we demonstrated that this method provides a wealth of information and has a number of advantages over other linear and nonlinear analysis techniques:

(i) It accurately detects the location of linear instabilities (when diffusivities are sufficiently different). It is however more than simply a scalable Turing analysis and provides different information.
(ii) It detects nonlinear patterning regimes where homogeneous steady states are linear stable and linear stability techniques fail to provide information.
(iii) In these regimes, it qualitatively characterizes the dependence of response thresholds on reaction parameters, a useful capability in biological applications.
(iv) The global bifurcation structure can be interpreted to provide reasonable conjectures about the type of pattern that might evolve on longer timescales.

The true value and power of this method however becomes evident in Sect. 5. There a biologically motivated system of nine chemotaxis regulators was investigated. With the help of readily available and relatively easy to use software, the same methodology and analysis that were employed in the much simpler earlier examples were applied without change in this case. This provided a concise, detailed overview of the parameter space structure of this complex model that no other method is capable of. Further, it allowed rapid investigation of the effects of both parameter and structural variations of the reaction network that yielded insights into the function of the system. For these reasons, the LPA has the potential to be of use in an array of scientific fields where RDEs arise.

Acknowledgements W.R.H. thanks Leah Edelstein-Keshet and Michael Ward as well as the anonymous reviewers for their valuable comments. This research was partially supported by the NIH grants R01 GM086882 (to Anders E. Carlsson and Leah Edelstein-Keshet) and P50 GM76516, and an NSERC discovery grant (to L.E.K.).

Appendix A: Schnakenberg Asymptotics

This analysis closely follows (Ward and Wei 2002). Consider the Schnakenberg system (11a), (11b) on the interval $[-1, 1]$. In Ward and Wei (2002), it was shown that

this system exhibits stable spike solutions when $a = 0$. That analysis can be extended to show such spikes in fact exist for all values of a under certain asymptotic conditions.

To begin, define

$$D = \frac{\bar{D}}{\epsilon}, \qquad v = \epsilon \bar{v}, \qquad u = \frac{\bar{u}}{\epsilon}, \tag{20}$$

and subsequently drop the $\bar{}$ to yield

$$u_t(x,t) = a\epsilon - u + u^2 v + \epsilon u_{xx}, \tag{21}$$

$$\epsilon v_t(x,t) = b - \frac{u^2 v}{\epsilon} + D v_{xx}, \tag{22}$$

Assuming $D \gg 1/\epsilon$, $v = v_0 + \epsilon v_1(x) + \cdots$, and integrating (22), it can be determined that

$$2b = \frac{v_0}{\epsilon} \int_{-1}^{1} u^2(x,t)\, dx. \tag{23}$$

A spike solution of the form $u(x) = u_0 + u_1(x/\epsilon)$ is now sought where u_0 and u_1 are the outer and inner solutions. It is assumed u_0 is spatially constant. Collecting terms involving the same powers of ϵ shows the outer solution is $u_0 \approx a\epsilon$ and the inner solution satisfies

$$u_1''(z) - u_1(z) + u_1^2(z) v_0 = 0 \tag{24}$$

on $x/\epsilon = z \in [-1, 1]$ with no flux boundary conditions. The solution to this problem is known (see Ward and Wei 2002) yielding

$$u(x) = u_0 + u_1 = a\epsilon + \frac{3}{2v_0} \operatorname{sech}^2\left(\frac{x}{2\epsilon}\right). \tag{25}$$

Integrating the square of this expression and substituting into (23) yields $v_0 = b/3$. Unravelling the change of coordinates yields the approximate spike solution for the original problem (Eqs. (11a), (11b)) on $[-1, 1]$

$$u(x) \approx a + \frac{b}{2\epsilon} \operatorname{sech}^2\left(\frac{x}{2\epsilon}\right), \qquad v(x) \approx \frac{3\epsilon}{b}. \tag{26}$$

So the Schnakenberg system (11a), (11b) in fact produces spike type solutions for all values of a in the limit $\epsilon \to 0$. This is in agreement with the results of the LPA in Fig. 2a and the progression of the fold bifurcation (where the spike is lost) to ∞ as $a \to \infty$ in the bifurcation analysis in Fig. 2c. Further, the maximum value of u in (26) with $a = 0$ compares to good precision with the maximum values shown at $a = 0$ in Fig. 2c, supporting these results.

Appendix B: Proof of Theorem 4.1

To prove Theorem 4.1, first notice the eigenvalues of J_k (18) can be segregated into two regions of the complex plane using the Gershgorin circle theorem (see Fig. 6).

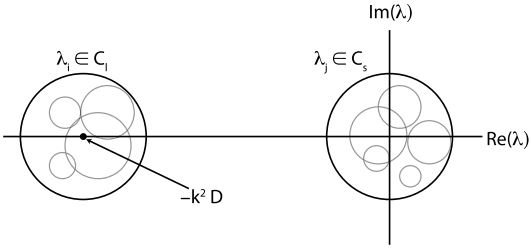

Fig. 6 Schematic of the separation of the eigenvalues of J_k in the complex plane. *Grey circles* indicate the different Gershgorin circles C_i. The *larger darker circles* indicate C_l and C_s, which contain all eigenvalues of J_k. These circles separate those eigenvalues into two classes with $O(1)$ and $O^-(D)$ real part, respectively

Fix a specific wave number k, let $a_{i,j}$ be the elements of J_k, and define

$$R_i = \sum_{j \neq i} |a_{i,j}|, \qquad C_i = C(a_{i,i}, R_i) \tag{27}$$

where $C(a, r)$ is the circle with center a and radius r. The Gershgorin circle theorem states that each eigenvalue of J_k lies in at least one of the disks C_i. The structure of J_k is such that the off diagonal entries are $O(1)$ with respect to D. So $R = \max\{R_i\}$ is $O(1)$. The diagonal entries fall into two categories, those that are $O(1)$ (corresponding to the small diffusion entries), and those that are $-k^2 D + O(1)$ (corresponding to large diffusion entries). Define Ω_s to be the union of the disks C_i that are characterized by $O(1)$ diagonal entries and Ω_l as the union of disks characterized by $O(D)$ diagonal entries. Since these disks have a maximal radius R independent of D, there exists disks $C_l = C(-k^2 D, \kappa_l R)$ and $C_s = C(0, \kappa_s R)$ so that for constants $\kappa_{l,s}$ independent of D, $\Omega_s \subset C_s$ and $\Omega_l \subset C_l$. For sufficiently large D, C_s and C_l do not overlap and hence separate $\{\lambda^k\}$ into two sets (see Fig. 6).

So, for each i, either $\mathfrak{Re}(\lambda_i^k) = O^-(D)$, or $\mathfrak{Re}(\lambda_i^k) = O(1)$. Since $\det(J_k) = O(D^N)$, $\{\lambda_i^k\}_{i=M+1:M+N}$ must have $O^-(D)$ real part. Also note that the imaginary parts of all eigenvalues are constrained to be less than $\max\{\kappa_s, \kappa_l\}R$ so that $\mathfrak{Im}(\lambda_k^i) = O(1)$ for all i as well, so $|\lambda_i^k| = O(1)$ for $i = 1 : M$.

Eigenvalues of J_k are roots of the characteristic polynomial

$$\left|J_k - \lambda I\right| = \begin{vmatrix} f_u\left(u^s, v^s\right) - \left(k^2\epsilon^2 + \lambda\right)I & f_v\left(u^s, v^s\right) \\ g_u\left(u^s, v^s\right) & g_v\left(u^s, v^s\right) - \left(k^2 D + \lambda\right)I \end{vmatrix} = 0, \tag{28}$$

where I is a properly sized identity matrix. Let P and Q be the unitary matrices that diagonalize $f_u(u^s, v^s)$ and $g_v(u^s, v^s)$. Then in particular the diagonal entries of $P^{-1} f_u(u^s, v^s) P$ are $\{\lambda_j^{LP}\}$ and the entries of $Q^{-1} g_v(u^s, v^s) Q$ are $O(1)$. Define

$$T = \begin{bmatrix} P & 0 \\ 0 & Q \end{bmatrix}. \tag{29}$$

Table 2 *Model parameters:* Base parameter set for the model depicted in Fig. 5a and represented in Eqs. (34a)–(34d). The primary parameters of interest are I_{R1}, which represents a basel activation rate parameter for Rac, and f_2 which modulates the strength of inhibitory feedback from Rho to Rac

Parameter name	Value	Meaning
L_0	20 μm	Domain size
C_t, R_t, ρ_t	2.4, 7.5, 3.1 μM	Total levels of Cdc42, Rac, and Rho
$\hat{I}_c, \hat{I}_{R1}, \hat{I}_{R2}, \hat{I}_\rho$	2.95, 0.2, 0.2, 6.6 μM s^{-1}	Cdc42, Rac, and Rho activation rates
a_1, a_2, a_3	1.25, 1, 1.25 μM	Cdc42 and Rho half max inhibition levels
n	3	Hill coefficient for inhibitory connections
α	0.55 s^{-1}	Cdc42 dependent Rac activation
$\delta_C, \delta_R, \delta_\rho$	1 s^{-1}	GAP decay rates of activated Rho-proteins
I_{P1}	10.5 μM/s	PIP_1 input rate
δ_{P1}	0.21 s^{-1}	PIP_1 decay rate
$k_{\text{PI5K}}, k_{\text{PI3K}}, k_{\text{PTEN}}$	0.084, 0.00072, 0.432 μM^{-1} s^{-1}	Baseline conversion rates
k_{21}	0.021 s^{-1}	Baseline conversion rate
P_{3b}	0.15 μM	Typical level of PIP_3
D_m, D_c, D_P	0.1, 50, 5 $\mu m^2/s$	Diffusion Rates
f_2	1	Nondimensional feedback parameter

Then the eigenvalue problem translates to

$$\begin{vmatrix} \left[\lambda^{LP}\right] - k^2\epsilon^2 I - \lambda I & P^{-1} f_v Q \\ Q^{-1} g_u P & Q^{-1} g_v\left(u^s, v^s\right) Q - k^2 D I - \lambda I \end{vmatrix} = \begin{vmatrix} A1 & A2 \\ A3 & A4 \end{vmatrix} = 0 \tag{30}$$

where $[\lambda^{LP}]$ is the diagonal form of $f_u(u^s, v^s)$. Notice that $A1$, $A4$ are diagonal.

Now consider an eigenvalue λ whose real part is $O(1)$. In this case, the diagonal entries of $A4$ are $O^-(D)$ and it is nonsingular. It can thus be used to eliminate $A2$. After this is done, the eigenvalue problem becomes

$$\begin{vmatrix} \left[\lambda^{LP}\right] - k^2\epsilon^2 I + O\left(D^{-1}\right) - \lambda I & 0 \\ Q^{-1} g_u P & Q^{-1} g_v\left(u^s, v^s\right) Q - k^2 D I - \lambda I \end{vmatrix} = 0. \tag{31}$$

Since the bottom right block is nonsingular, it must be true that

$$\det\left(\left[\lambda^{LP}\right] - k^2\epsilon^2 I + O\left(D^{-1}\right) - \lambda I\right) = 0. \tag{32}$$

where $O(D^{-1})$ is a properly sized matrix with entries of this size. With $D = \infty$, the roots of this polynomial are simply $\{\lambda_j^{LP} - k^2\epsilon^2\}$. It is tempting to view Eq. (32) as a perturbation of this case and apply some form of perturbation bound. However, f_u is not Hermitian, which is usually required for such bounds. Instead, the best we can say is that by continuity of the determinant, the roots of this polynomial satisfy

$$\lambda = \lambda_j^{LP} - k^2\epsilon^2 + c(D), \tag{33}$$

where $c(D) \to 0$ as $D \to \infty$.

Appendix C: GTPase Model Equations

Figure 5a schematically diagrams interactions between three interacting GTPases and three phosphoinositides. I briefly outline the model equations describing these interactions. Further specifics can be found in Holmes et al. (2012b), Lin et al. (2012). Modifications of the model presented in those references, which are the subject of investigation here, are described in the main text. Each GTPase undergoes conservative cycling between active membrane bound and inactive forms in the cell interior by (un)binding to the membrane. These dynamics are described by

$$\begin{aligned}\frac{\partial G}{\partial t} &= I_G \frac{G^c}{G_t} - \delta_G G + D_m G_{xx},\\ \frac{\partial G^c}{\partial t} &= -I_G \frac{G^c}{G_t} + \delta_G G + D_c G^c_{xx},\end{aligned} \tag{34a}$$

where $G = R, \rho, C$ represents the membrane bound form and G^c represents an inactive cytosolic form. Phosphoinositides interconvert between three states through the hydrolysis/phosphorylation activity of PI5K, PI3K, PTEN, etc., which are not explicitly modeled. The GTPase activation rate functions encoding the interactions in Fig. 5a are defined by

$$\begin{aligned}I_C &= \left(\frac{\hat{I}_C}{1+(\rho/a_1)^n}\right), \qquad I_R = \left(\hat{I}_{R1} + \frac{\alpha C + \hat{I}_{R2}\frac{P_3}{P_{3b}}}{1+f_2(\rho/a_3)^n}\right),\\ I_\rho &= \frac{\hat{I}_\rho}{1+(R/a_2)^n}.\end{aligned} \tag{34b}$$

Phosphoinositide kinetics are modeled by linear and mass action kinetics

$$\begin{aligned}\frac{\partial P_1}{\partial t} &= I_{P1} - \delta_{P1} P_1 + k_{21} P_2 - f_{\text{PI5K}}(R,C,\rho) P_1 + D_P P_{1xx},\\ \frac{\partial P_2}{\partial t} &= -k_{21} P_2 + f_{PI5K}(R,C,\rho) P_1 - f_{\text{PI3K}}(R,C,\rho) P_2\\ &\quad + f_{\text{PTEN}}(R,C,\rho) P_3 + D_P P_{2xx},\\ \frac{\partial P_3}{\partial t} &= f_{\text{PI3K}}(R,C,\rho) P_2 - f_{\text{PTEN}}(R,C,\rho) P_3 + D_P P_{3xx},\end{aligned} \tag{34c}$$

with feedback terms

$$\begin{aligned}f_{\text{PI3K}} &= \frac{k_{\text{PI3K}}}{2}\left(1+\frac{R}{R_t}\right), \quad f_{\text{PI5K}} = \frac{k_{\text{PI5K}}}{2}\left(1+\frac{R}{R_t}\right),\\ f_{\text{PTEN}} &= \frac{k_{\text{PTEN}}}{2}\left(1+\frac{\rho}{\rho_t}\right).\end{aligned} \tag{34d}$$

See Table 2 for a base parameter set for this model.

References

Barrass, I., Crampin, E. J., & Maini, P. K. (2006). Mode transitions in a model reaction–diffusion system driven by domain growth and noise. *Bull. Math. Biol.*, *68*, 981–995.

Caron, E. (2003). Rac signalling: a radical view. *Nat. Cell Biol.*, *5*, 185–187.

Crampin, E. J., Gaffney, E. A., & Maini, P. K. (1999). Reaction and diffusion on growing domains: scenarios for robust pattern formation. *Bull. Math. Biol.*, *61*, 1093–1120.

Dawes, A. T., & Edelstein-Keshet, L. (2007). Phosphoinositides and rho proteins spatially regulate actin polymerization to initiate and maintain directed movement in a one-dimensional model of a motile cell. *Biophys. J.*, *92*, 744–768.

Dhooge, A., Govaerts, W., & Kuznetsov, Yu. A. (2003). Matcont: a matlab package for numerical bifurcation analysis of odes. *ACM Trans. Math. Softw.*, *29*, 141–164. doi:10.1145/779359.779362

Doelman, A., & Veerman, F. (2012). An explicit theory for pulses in two component singularly perturbed reaction-diffusion equations. *J. Dyn. Diff. Equ.* doi:10.1007/s10884-013-9325-2.

Doedel, E., Champneys, A., Fairgrieve, T., Kuznetsov, Y., Oldeman, B., Paffenroth, R., Sandstede, B., Wang, X., & Zhang, C. (2007). Auto-07p: continuation and bifurcation software for ordinary differential equations: Continuation and bifurcation software for ordinary differential equations, URL http://indy.cs.concordia.ca/auto.

Doelman, A., Gardner, R. A., & Kaper, T. J. (1998). Stability analysis of singular patterns in the 1D Gray–Scott model: a matched asymptotics approach. *Physica D*, *122*, 1–36.

Doelman, A., Kaper, T. J., & Promislow, K. (2007). Nonlinear asymptotic stability of the semistrong pulse dynamics in a regularized Gierer–Meinhardt model. *SIAM J. Math. Anal.*, *38*, 1760–1787.

Ferguson, G. J., Milne, L., Kulkarni, S., Sasaki, T., Walker, S., Andrews, S., Crabbe, T., Finan, P., Jones, G., Jackson, S., et al. (2006). Pi (3) $k\gamma$ has an important context-dependent role in neutrophil chemokinesis. *Nat. Cell Biol.*, *9*, 86–91.

Fu, Y., & Yang, Z. (2001). Rop gtpase: a master switch of cell polarity development in plants. *Trends Plant Sci.*, *6*, 545–547.

Gierer, A., & Meinhardt, H. (1972). A theory of biological pattern formation. *Kybernetik*, *12*, 30–39.

Goehring, N. W., Trong, P. K., Bois, J. S., Chowdhury, D., Nicola, E. M., Hyman, A. A., & Grill, S. W. (2011). Polarization of par proteins by advective triggering of a pattern-forming system. *Science*, *334*, 1137–1141.

Grieneisen, V. (2009). *Dynamics of auxin patterning in plant morphogenesis*. PhD thesis, University of Utrecht.

Holmes, W. R., Carlsson, A. E., & Edelstein-Keshet, L. (2012a). Regimes of wave type patterning driven by refractory actin feedback: transition from static polarization to dynamic wave behavior. *Phys. Biol.*, *9*, 046005.

Holmes, W. R., Lin, B., Levchenko, A., & Edelstein-Keshet, L. (2012b). Modeling cell polarization driven by synthetic spatially graded rac activation. *PLoS Comput. Biol.*, *8*, e1002366.

Huang, K. C., Meir, Y., & Wingreen, N. S. (2003). Dynamic structures in *Escherichia coli*: spontaneous formation of mine rings and mind polar zones. *Proc. Natl. Acad. Sci. USA*, *100*, 12724–12728.

Huang, K. C., & Wingreen, N. S. (2005). Min-protein oscillations in round bacteria. *Phys. Biol.*, *1*, 229.

Iron, D., & Ward, M. J. (2000). A metastable spike solution for a nonlocal reaction diffusion model. *SIAM J. Appl. Math.*, *60*, 778–802.

Iron, D., Wei, J., & Winter, M. (2004). Stability analysis of turing patterns generated by the Schnakenberg model. *J. Math. Biol.*, *49*, 358–390.

Jilkine, A., & Edelstein-Keshet, L. (2011). A comparison of mathematical models for polarization of single eukaryotic cells in response to guided cues. *PLoS Comput. Biol.*, *7*, e1001121.

Jilkine, A., Marée, A. F. M., & Edelstein-Keshet, L. (2007). Mathematical model for spatial segregation of the rho-family GTPases based on inhibitory crosstalk. *Bull. Math. Biol.*, *69*, 1943–1978.

Kaper, H. G., Wang, S., & Yari, M. (2009). Dynamical transitions of Turing patterns. *Nonlinearity*, *22*, 601.

Kernevez, J. P., Joly, G., Duban, M. C., Bunow, B., & Thomas, D. (1979). Hysteresis, oscillations, and pattern formation in realistic immobilized enzyme systems. *J. Math. Biol.*, *7*, 41–56.

Kolokolnikov, T., Ward, M. J., & Wei, J. (2005a). The existence and stability of spike equilibria in the one-dimensional Gray–Scott model: the low feed-rate regime. *Stud. Appl. Math.*, *115*, 21–71.

Kolokolnikov, T., Ward, M. J., & Wei, J. (2005b). The existence and stability of spike equilibria in the one-dimensional gray Scott model: the pulse-splitting regime. *Physica D*, *202*, 258–293.

Kolokolnikov, T., Ward, M. J., & Wei, J. (2005c). Pulse-splitting for some reaction-diffusion systems in one-space dimension. *Stud. Appl. Math.*, *114*, 115–165.

Lewis, M. A., & Kareiva, P. (1993). Allee dynamics and the spread of invading organisms. *Theor. Popul. Biol.*, *43*, 141–158.

Li, F., & Ni, W. M. (2009). On the global existence and finite time blow-up of shadow systems. *J. Differ. Equ.*, *247*, 1762–1776.

Lin, B., Holmes, W. R., Wang, C. J., Ueno, T., Harwell, A., Edelstein-Keshet, L., Inoue, T., & Levchenko, A. (2012). Synthetic spatially graded rac activation drives cell polarization and movement. In *Proceedings of the national academy of sciences, early edition*.

Marée, A. F. M., Jilkine, A., Dawes, A., Grieneisen, V. A., & Edelstein-Keshet, L. (2006). Polarization and movement of keratocytes: a multiscale modelling approach. *Bull. Math. Biol.*, *68*, 1169–1211.

Mata, M. A., Dutot, M., Edelstein-Keshet, L., & Holmes, W. R. (2013). A model for intracellular actin waves explored by nonlinear local perturbation analysis. *J. Theor. Biol.*, *334*, 149–161.

Mori, Y., Jilkine, A., & Edelstein-Keshet, L. (2008). Wave-pinning and cell polarity from a bistable reaction–diffusion system. *Biophys. J.*, *94*, 3684–3697.

Mori, Y., Jilkine, A., & Edelstein-Keshet, L. (2011). Asymptotic and bifurcation analysis of wave-pinning in a reaction–diffusion model for cell polarization. *SIAM J. Appl. Math.*, *71*, 1401–1427.

Murray, J. D. (1982). Parameter space for Turing instability in reaction diffusion mechanisms: a comparison of models. *Journal of Theoretical Biology*, 143–163.

Murray, J. D. (2002). *Mathematical biology: an introduction*. *Interdisciplinary applied mathematics* (3rd ed.). Berlin: Springer.

Nishiura, Y. (1982). Global structure of bifurcating solutions of some reaction–diffusion systems. *SIAM J. Appl. Math.*, *13*, 555–593.

Pismen, L. M., & Rubinstein, B. Y. (1999). Computer tools for bifurcation analysis: general approach with application to dynamical and distributed systems. *Int. J. Bifurc. Chaos Appl. Sci. Eng.*, *9*, 983–1008.

Rodrigues, L. A. D., Mistro, D. C., & Petrovskii, S. (2011). Pattern formation, long-term transients, and the Turing–Hopf bifurcation in a space-and time-discrete predator–prey system. *Bull. Math. Biol.*, *73*, 1812–1840.

Rubinstein, B., Slaughter, B. D., & Li, R. (2012). Weakly nonlinear analysis of symmetry breaking in cell polarity models. *Phys. Biol.*, *9*, 045006.

Sander, E. E., Jean, P., Van Delft, S., Van Der Kammen, R. A., & Collard, J. G. (1999). Rac downregulates rho activity reciprocal balance between both gtpases determines cellular morphology and migratory behavior. *J. Cell Biol.*, *147*, 1009–1022.

Schnakenberg, J. (1979). Simple chemical reaction systems with limit cycle behavior. *J. Theor. Biol.*, *81*, 389–400.

Short, M. B., Bertozzi, A. L., & Brantingham, P. J. (2010). Nonlinear patterns in urban crime: hotspots, bifurcations, and suppression. *SIAM J. Appl. Dyn. Syst.*, *9*, 462–483.

Turing, A. M. (1952). The chemical basis of morphogenesis. *Philos. Trans. R. Soc. Lond. B, Biol. Sci.*, *237*, 37–72.

Ueda, K. I., & Nishiura, Y. (2012). A mathematical mechanism for instabilities in stripe formation on growing domains. *Physica D*, *241*, 37–59.

van der Stelt, S., Doelman, A., Hek, G., & Rademacher, J. D. M. (2013). Rise and fall of periodic patterns for a generalized Klausmeier–Gray–Scott model. *J. Nonlinear Sci.*, *23*, 39–95.

van Leeuwen, F. N., Kain, H. E. T., van der Kammen, R. A., Michiels, F., Kranenburg, O. W., & Collard, J. G. (1997). The guanine nucleotide exchange factor tiam1 affects neuronal morphology; opposing roles for the small gtpases rac and rho. *J. Cell Biol.*, *139*, 797–807.

Veerman, F., & Doelman, A. (2013). Pulses in a Gierer–Meinhardt equation with a slow nonlinearity. *SIAM J. Appl. Dyn. Syst.*, *12*, 28–60.

Wang, W., Liu, Q., & Jin, Z. (2007). Spatiotemporal complexity of a ratio-dependent predator–prey system. *Phys. Rev. E*, *75*, 051913.

Ward, M. J., & Wei, J. (2002). The existence and stability of asymmetric spike patterns for the Schnakenberg model. *Stud. Appl. Math.*, *109*, 229–264.